Sensors and Actuators B 194 (2014) 229–237

Contents lists available at ScienceDirect

Sensors and Actuators B: Chemical

journal homepage: www.elsevier.com/locate/snb

Naked eye and fluorescent detections of Hg^{2+} ions and Cysteine via *J*-aggregation and deaggregation of a perylene bisimide derivative

Hsiao-Ping Fang, Muthaiah Shellaiah, Ashutosh Singh, Mandapati V. Ramakrishnam Raju, Yen-Hsing Wu, Hong-Cheu Lin *

Department of Materials Science and Engineering, National Chiao Tung University, Hsinchu, Taiwan

ARTICLE INFO

Article history:
Received 23 October 2013
Received in revised form
17 December 2013
Accepted 20 December 2013
Available online 31 December 2013

Keywords:
Perylene bisimide
Hg^{2+} mediated Cys sensor
J-Aggregation and deaggregation
Reversible sensor
TRPL spectra

ABSTRACT

Selective naked eye and fluorescent sensor responses of a 1,6,7,12-tetra(4-*tert*-butylphenoxy)perylene-3,4:9,10-tetracarboxylic acid bisimide (**PBI**) derivative are reported for the first time toward Hg^{2+} ions and Cysteine (Cys) via *J*-aggregation and deaggregation mechanisms. The *J*-aggregation and deaggregation of **PBI** induced by Hg^{2+} and Cys were well established by UV–vis/PL and ^{1}H NMR titrations. The 1:1 stoichiometry of **PBI**-Hg^{2+} and Cys-Hg^{2+}/**PBI** ensembles were elucidated from the jobs plots based on their UV–vis spectral changes. The linear complex formation by **PBI**-Hg^{2+} ensemble was confirmed through FT-IR and ^{1}H NMR spectral studies and well supported by its reversible nature upon the addition of pentamethyl diethylene triamine (PMDTA). The positive cooperativities of Hg^{2+} and Cys (with **PBI**) in **PBI**-Hg^{2+} and Cys-Hg^{2+}/**PBI** ensembles were evidenced from the Hill plots based on their fluorescence binding isotherms. The detection limits of Hg^{2+} ions and Cys were calculated as 36.6 and 91.3 nM, respectively, by standard deviations and linear fittings of their Stern–Volmer (K_{SV}) constants and relative fluorescence intensity changes, respectively. Furthermore, the sensor properties of **PBI** were well investigated by K_{SV} constants, pH values, time effects, and time resolved photoluminescence (TRPL) spectra.

1. Introduction

Attributed to the inherent toxic effects on human health and environment, the design and development of chemical sensors for mercury ions become a topic of recent concern [1–5]. In the middle of the most toxic metals, mercury is the one widespread in air, water, and soil, generated by sources like gold productions, coal plants, thermometers, barometers, caustic soda and mercury lamps [6–14]. Mercury contaminations can cause strong damage to the central nervous system, and its accumulations in the human body may lead to various cognitive, motor disorders, and Minamata disease [15–18]. Since the major mercury absorption source is related to daily diet, such as fish [19], there are significant efforts contributed to the developments of the selective and sensitive detections of mercury [20,21]. Chemodosimeters with specific binding interactions between analytes and probe molecules gained a great deal of interests in recent years owing to their specific chemical interactions with the targets of interests, such as toxic transition metals and neutral small molecules [22]. Despite of their pervasive advantages in bio-imaging and specific low detection limits, chemodosimeters often rely on specific covalent interactions with long response time [23]. Orthodoxly, chemosensing ensemble approaches are known to act as ideal sensing plat-forms; owing to their ease in detections with a positive cooperative non-covalent interactions [24]. According to the high toxicity point of view for mercury; many groups across the world are doing their researches to detect mercury at low levels. Recently Yi Zhou et al. published fluorescent sensor for detection of Hg^{2+} metal ion with a detection limit 4.34 mol L^{-1} [14].

On the other hand, due to their structural and functional importance, thiol-based amino acids play crucial roles in biological systems [25–28] and also act as indicators of diseases like Alzheimer's, AIDS, and cancers [29–33]. Among them, L-Cysteine (Cys) plays a very important role in protein folding [34] and its deficiency would lead to many diseases, such as hematopoiesis decrease, leukocyte loss, psoriasis, etc. [35–38]. Hence, the developments of sensory probes for Cys are still highly demanded.

Owing to the importance of mercury ions and Cys, many sensory reports with different detection methods (neutron activation analysis, ion sensitivity, flame photometry, electron microprobe analysis and spectroscopic methods) are available for them [39–42]. However, due to the simplicity, high degrees of specificity and low detection limits, many colorimetric (naked eye) and fluorescent sensors for mercury ions and Cys were developed with diverse mechanisms [43–51]. Among them, metal complexes mediated fluorescent "turn-on" sensors for Cys [52–54] were

* Corresponding author at: Department of Materials Science and Engineering, National Chiao Tung University, Hsinchu, Taiwan, ROC. Tel.: +886 3 5712121x55305; fax: +886 3 5724727.
E-mail address: linhc@mail.nctu.edu.tw (H.-C. Lin).

0925-4005/$ – see front matter © 2013 Elsevier B.V. All rights reserved.
http://dx.doi.org/10.1016/j.snb.2013.12.082

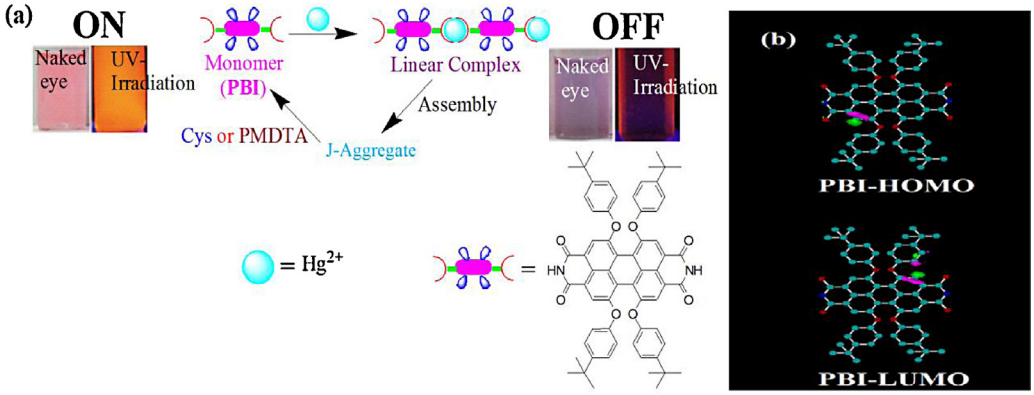

Fig. 1. (a) Schematic representations for Hg^{2+}-induced *J*-aggregation of **PBI** and aggregate dissociation in the presence of Cys or PMDTA and (b) computation analysis of HOMO and LUMO levels of **PBI** (semi-empirical PM3 method).

more attractive. More interestingly, Jiang et al. reported the Hg^{2+} mediated Cys sensor through perylene bisimide (**PBI**) based on aggregation and deaggregation mechanisms [55]. Furthermore, the report motivated just to fluorescent detections of Hg^{2+} ions and Cys via H-aggregation and deaggregation of **PBI**.

Since many **PBI** derivatives were known as colored compounds with improved solubilities and also can aggregate (H or J) [56–60], we made an attempt to report the sensor responses of a well-known **PBI** derivative (i.e., 1,6,7,12-tetra(4-*tert*-butylphenoxy)perylene-3,4:9,10-tetracarboxylic acid bisimide) for naked eye and fluorescent detections of Hg^{2+} and Cysteine via *J*-aggregation and deaggregation. Remarkably, in contrast to the previous report [55], the *J*-aggregation of the **PBI** derivative were evidenced to be induced by Hg^{2+} ions via "T–Hg^{2+}–T" like binding motif of its imide groups (similar to the binding site of thymine (T)) by bathochromic shifts of UV/PL spectra. Similarly, upon the addition of Cys the *J*-aggregation of **PBI**-Hg^{2+} ensemble deaggregates through strong Hg^{2+}–S interactions and provides the monomeric spectra as noted in the schematic representation of Fig. 1a.

Herein, we report a **PBI** derivative for naked eye and fluorescent detections of Hg^{2+} ions and Cysteine via *J*-aggregation induced by Hg^{2+} ions and deaggregation by Hg^{2+}–S interactions of Cys.

2. Experimental

2.1. Materials

All anhydrous reactions were carried out by standard procedures under nitrogen atmosphere to avoid moisture. The solvents were dried by distillation over appropriate drying agents. Reactions were monitored by TLC plates and column chromatography was generally performed on silica gel. ^1H and ^{13}C NMR were recorded on a 300 MHz spectrometer. The chemical shifts (δ) are reported in ppm and coupling constants (*J*) in Hz and relative to TMS (0.00) for ^1H and ^{13}C NMR, (s, d, t, q, m, and br mean single, double, ternary, quadruple, multiple, and broad single, respectively), and D-chloroform (7.26 ppm) and (77.0 ppm) was used as references for ^1H and ^{13}C NMR, respectively. Mass spectra (FAB) were obtained on the respective mass spectrometer. Elemental analysis was carried out by Elemental Vario EL. Absorption and fluorescence spectra were measured on V-670 spectrophotometer and F-4500 fluorescence spectrophotometer, respectively. Time-resolved photoluminescence (TRPL) spectra were measured using a home-built single photon counting system. Excitation was performed using a 565 nm diode laser (Picoquant PDL-200, 50 ps FWHM, 2 MHz). The signals collected at the excitonic emissions of solutions were connected to a time-correlated single photon counting card (TCSPC, Picoquant Timeharp 200). The emission decay data were analyzed with the biexponential kinetics in which two decay components were derived. The lifetime values (τ_1 and τ_2) and pre-exponential factors (A_1 and A_2) were determined and summarized. 1–14 pH buffers were freshly prepared as per the literature [61].

2.2. Sensor titrations

PBI was dissolved in THF:H_2O (2:1) at 1×10^{-6} M concentration. Li^+, Ag^+, K^+, Na^+, Cs^+, Ni^{2+}, Fe^{3+}, Co^{2+}, Zn^{2+}, Cd^{2+}, Pb^{2+}, Ca^{2+}, Cr^{3+}, Mg^{2+}, Cu^{2+}, Mn^{2+}, Hg^{2+}, Ag^{2+}, Cu^+, Sn^{2+}, Eu^{3+}, Ba^{2+} and Al^{3+} metal cations were dissolved in water medium at 1×10^{-4} M concentration from their respective chloro compounds, and Ag^+, Mn^{2+}, Eu^{3+}, Hg^{2+} and Mg^{2+} were made from $AgNO_3$, $Mn(OAc)_2$, $Eu(OAc)_3$, $Hg(OAc)_2$ and $MgSO_4$, respectively, in water medium at 1×10^{-5} M concentration. Metal ion mixtures contained all above ions, except Hg^{2+}. Penta methyl diethylene triamine (PMDTA) was dissolved in THF at 1×10^{-5} M.

2.3. NMR titrations

10 mmol (1 equiv.) of **PBI** in THF-d8 was titrated with 10 mmol (1 equiv.) of Hg^{2+} in D_2O and also titrated with 10 mmol (1 equiv.) of Cys in D_2O.

2.4. Synthesis of 1,6,7,12-tetra(4-tert-butylphenoxy)perylene-3,4:9,10-tetracarboxylic acid bisimide (*PBI*)

All the intermediates were synthesized as per the required purities and **PBI** probe also synthesized according to the literature procedure as mentioned in Section 3.1; ^1H NMR (300 MHz, $CDCl_3$), δ 1.29 (s, 36H, $C(CH_3)_3$), 6.80 (d, 8H, J = 9 Hz, ArH), 7.22 (d, J = 9 Hz, ArH), 8.21 (s, 4H, -Peri ArH), 8.46 (s, 2H, —NH)). ^{13}C NMR (75 MHz, $CDCl_3$) δ 31.43, 34.38, 119.29, 119.60, 120.86, 122.30, 126.73, 147.49, 152.71, 155.98, 162.99. (FAB): 983 (M+, 100%), Anal. Calcd for $C_{64}H_{58}N_2O_8$: C, 78.19; H, 5.95; N, 2.85. Found: C; 78.56; H, 5.90; N, 2.82.

3. Results and discussion

3.1. Synthesis and HOMO and LUMO levels of *PBI*

The **PBI** probe was synthesized (see Scheme S1) as per the literature reports [62–64] with a high purity and an overall yield of 77%, and fully characterized by ^1H- and ^{13}C NMR, along with mass (FAB) spectra (Figs. S1–S3). Insertion of phenoxy group in the perylene unit provided enough structural possibilities of forming the *J*-aggregation with Hg^{2+} and water. Furthermore, the HOMO–LUMO calculation of **PBI** was carried out by semi-empirical PM3 method

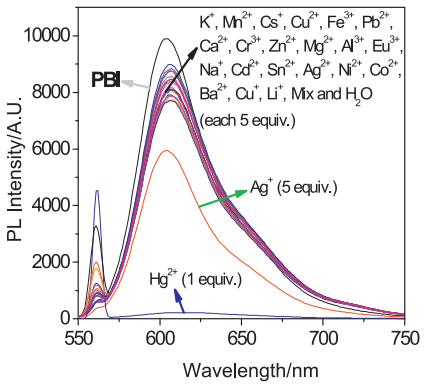

Fig. 2. Sensor responses of **PBI** (1 μM) in THF:H_2O (2:1) toward various metal ions in H_2O (λ_{ex} = 562 nm).

[65]. The schematic representations for Hg^{2+}-induced *J*-aggregation of **PBI** and aggregate dissociation in the presence of Cys or PMDTA are demonstrated in Fig. 1a. As shown in Fig. 1b, the HOMO electron clouds located toward one of the imide bonds and LUMO electron clouds were positioned between the phenyl ring of the phenoxy moiety and perylene ring near imide bond. The HOMO and LUMO levels of PBI well supported the electron/energy transfer from PBI to Hg^{2+} ions to form the linear *J*-aggregated complex assembly, and as well as the presence of π–π stacking in PBI.

3.2. Solvent selection for sensor titrations

PBI exhibited the absorption and PL maxima at 562 and 591 nm, respectively, in THF (Table 1). Furthermore, as noticed in Figs. S4 and S5, while increasing the water concentration (0–99% vol.), the PL intensities and quantum yield (Φ) values decreased rapidly among 60–99% (in vol.) of water concentrations. However, the bathochromic shifts of PL spectra also confirmed the *J*-aggregated assembly of PBI induced by water and hence supported the *J*-aggregation induced by Hg^{2+} ions. Even though, as shown in Table 1 and Fig. S4, the PL spectra and Φ values of PBI were not affected up to 1:1 vol. ratio of THF:H_2O. To avoid the confusion between water-induced quenching and metal ion-induced quenching, we performed the UV–vis/PL sensor titrations of PBI in THF:H_2O (2:1 in vol.) and metal ions as well as amino acids in H_2O. Similarly, ^1H NMR titrations were carried out by dissolving **PBI** in THF-d8 along with Hg^{2+} ions and Cys in D_2O. In the beginning, we performed the sensor titrations at pH = 7 and later on, evaluated our decision by the pH effects on Hg^{2+} sensor responses.

3.3. Fluorescence titrations on metal ions

The PL spectra of **PBI** were acquired by the excitation wavelength of 562 nm, where the maximum absorbance of **PBI** was observed [60,68]. Initially, **PBI** (1 μM) in THF:H_2O (2:1) was investigated toward 5 μM (5 equiv.) of metal ions (Li^+, Ag^+, K^+, Na^+, Cs^+, Ni^{2+}, Fe^{3+}, Co^{2+}, Zn^{2+}, Cd^{2+}, Pb^{2+}, Ca^{2+}, Cr^{3+}, Mg^{2+}, Cu^{2+}, Mn^{2+}, Hg^{2+}, Ag^{2+}, Cu^+, Sn^{2+}, Eu^{3+}, Ba^{2+} and Al^{3+}) in H_2O. As noticed in Fig. 2, **PBI** showed a better selectivity to Hg^{2+} ions, with a rapid fluorescence quenching in contrast to the other ions. However, further analysis was also confirmed that just 1 μM (1 equiv.) of Hg^{2+} ions could quench **PBI** completely as noticed in Fig. 2. In addition to the above PL spectral evidence, the better selectivity of **PBI** toward Hg^{2+} ions was confirmed by the fluorescence quenched by Hg^{2+} and other metal ions. More interestingly, the selectivity of **PBI** to Hg^{2+} ions was well notified with naked eye colorimetric change (pink to dark blue) as publicized Fig. 3. The better selectivity of **PBI** toward Hg^{2+} was further demonstrated by the single

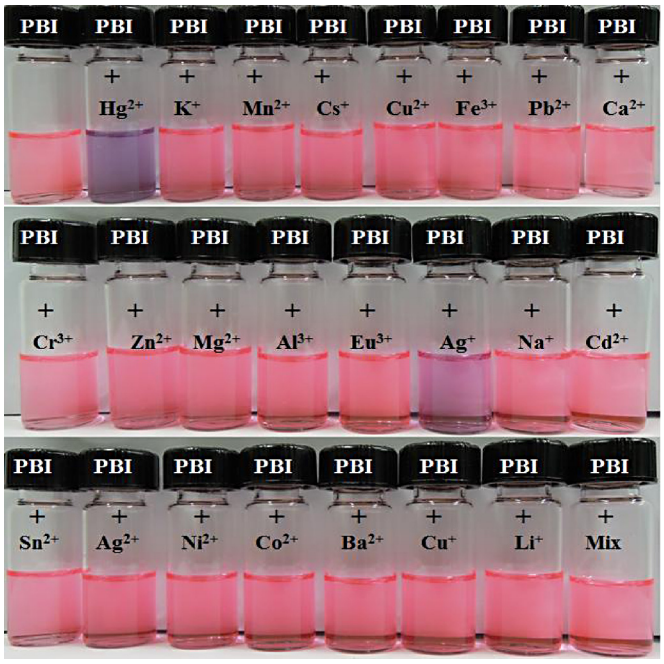

Fig. 3. Photographs of naked eye sensor responses of **PBI** (1 equiv.) toward Hg^{2+} (1 equiv.) and other metal ions (5 equiv.). (For interpretation of the references to color in this text, the reader is referred to the web version of the article.)

and dual metal analysis as shown in Figs. 4 and S6. Except Hg^{2+}, none of the other ions provided the fluorescence or colorimetric changes upon the addition of 1 equiv. of metal ions. However, Ag^+ showed a mild effect at an excess addition (5 equiv.) as visualized in Fig. 3. Similar to the single metal analysis, a better selectivity of **PBI** to Hg^{2+} ions was also evidenced in dual metal analysis, in which 1 equiv. (1 μM) of Hg^{2+} was mixed with 1 equiv. (1 μM) of background metal ions. Figs. 4 and S6 were evidenced the better selectivities of **PBI** toward Hg^{2+} ions and the Stern–Volmer quenching constant (K_{SV}) calculations also confirmed the above statement. The K_{SV} values were calculated by $K_{SV} = (I/I_0 - 1)/[Q]$; [Q], quencher concentration (1 μM for all metal ions), and the K_{SV} value of Hg^{2+}-**PBI** was evidenced as 4.68×10^7 M^{-1}. As shown in Table S1, except Hg^{2+} none of the remaining metal ions showed better K_{SV} values and hence confirmed the superior selectivity of **PBI** to form the *J*-aggregated Hg^{2+}-**PBI** ensemble. To evaluate the formation of *J*-aggregated Hg^{2+}-**PBI** ensemble and the deaggregation induced by Cys, we continued the titration experiments separately with Hg^{2+} and amino acids as follows.

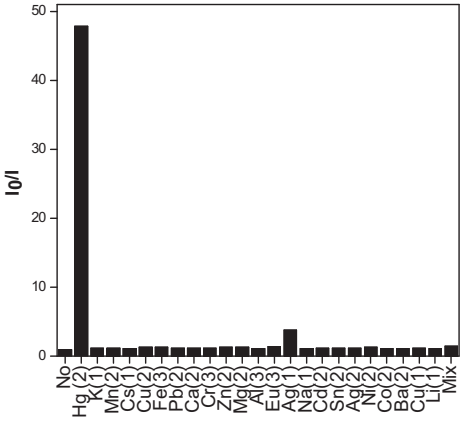

Fig. 4. Relative fluorescence intensity changes of **PBI** (1 μM) in THF:H_2O (2:1) mixed with 1 equiv. (1 μM) of various metal ions in H_2O (λ_{ex} = 562 nm).

Table 1
Photophysical and sensor properties of **PBI**.

Compound	Quantum yield (Φ)	log K_{app}[e]	Detection limits (LODs)[f]	τ (ns)[g]
PBI (λ_{ex} = 562 and λ_{em} = 591 nm)	0.55[a] 0.50[b] 0.36[c] 0.03[d]	NA	NA	5.59
PBI+Hg^{2+} (λ_{ex} = 562 and λ_{em} = 612 nm)	0.03	27.7	36.6 nM	2.37
PBI+Hg^{2+}+Cys (λ_{ex} = 562 and λ_{em} = 591 nm)	0.52	9.2	91.3 nM	5.16
PBI+Hg^{2+}+PMDTA (λ_{ex} = 562 and λ_{em} = 591 nm)	0.53	NA	NA	5.37

[a] THF.
[b] THF:H_2O (1:1).
[c] THF:H_2O (2:3).
[d] THF:H_2O (1:99), and rhodamine G in ethanol as a reference standard (Φ = 0.95).
[e] log K_{app} calculated from hill plots based on fluorescence spectral changes.
[f] LODs calculated by standard deviations and linear fittings.
[g] Fluorescence lifetime values.

3.4. Fluorescence titrations on Hg^{2+} and amino acids

By increasing the concentrations of Hg^{2+} (0–1000 nM with an equal span of 100 nM in H_2O), the sensitivity of **PBI** (1 μM) in THF:H_2O (2:1) toward Hg^{2+} ions was clearly observed in Fig. S7a via red-shifted fluorescence quenching. Initially, **PBI** exhibited the fluorescence peak at 591 nm and during the increment addition of Hg^{2+} ions to **PBI**, the peaks were slowly shifted for each addition with quenching and completely quenched at 612 nm as revealed in Table 1 and Fig. S7. The above observation and UV–vis spectral changes (Fig. 5a) of **PBI** with Hg^{2+} were also verified the formation of *J*-aggregation by **PBI**-Hg^{2+} ensemble. As noticed in Fig. 5a, the UV–vis spectra of **PBI** bathochromically shifted from 562 to 583 nm, but its intensity was slowly quenched over the addition of 1 μM of Hg^{2+}. The isosbestic point at 565 nm in absorption spectra was due to the interaction of Hg^{2+} with **PBI** and hence, confirmed the formation of *J*-aggregated **PBI**-Hg^{2+} ensemble. Furthermore, the **PBI**-Hg^{2+} linear complex formation was supported by the IR-spectral changes of **PBI** and **PBI**-Hg^{2+} (Fig. S8), in which the imide —NH peak at 3172 cm^{-1} utterly disappeared along with spectral shift of imide —C=O group (from 1698, 1678 cm^{-1} to 1623, 1602 cm^{-1}, respectively). Later on, the linear **PBI**-Hg^{2+} complex formation was also further supported by ^1H NMR titrations of **PBI** with Hg^{2+}. As revealed in Section 1, in contrast to Jiang et al. report, **PBI** provided the *J*-aggregated assembly with Hg^{2+} ions, therefore we extended our work toward amino acids to check the reversibility of the linear aggregated assembly.

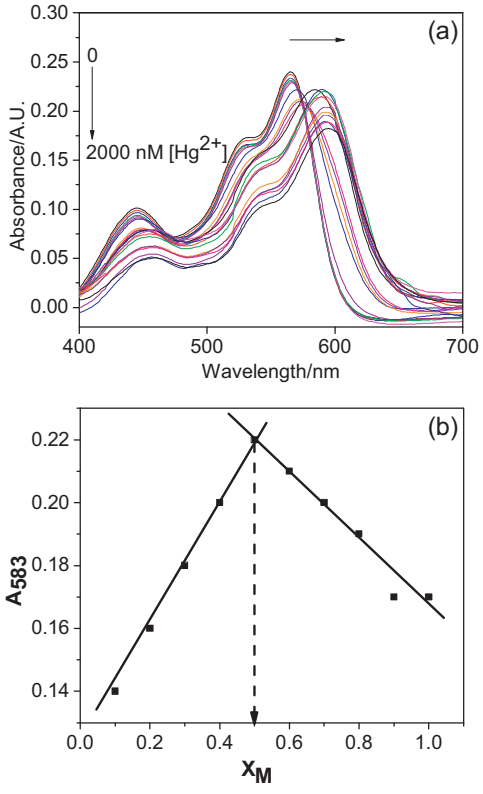

Fig. 5. (a) UV–vis spectra of **PBI** as a function of Hg^{2+} ions (0.1–2 μM) (b) Job plots of complex **PBI**-Hg^{2+}; $X_M = [M^{n+}]/[M^{n+}] + \mathbf{PBI}$, **PBI**-$Hg^{2+}$ = 1:1 stoichiometry (ca. 0.503).

As shown in Fig. S9a, the reversibility of **PBI**-Hg^{2+} ensemble was screened with available amino acids, such as Leucine (Leu), Tyrosine (Tyr), Glutamic acid (Glu), Aspartic acid (Asp), Lysine (Lys), Phenyl alanine (Phe), Histidine (His), L-Proline (Pro), Glycine (Gly) and L-Cysteine (Cys) in H_2O. Among the above amino acids, Cys provided a reversible monomeric PL peak of **PBI** at 591 nm via deaggregation of **PBI**-Hg^{2+} ensemble. However, we found a complete recovery of **PBI** peak by 2 equiv. (2 μM) addition of Cys in H_2O. The relative fluorescence intensity changes of **PBI**-Hg^{2+} ensemble with amino acids in H_2O was evidenced in Fig. S9b and confirmed the selective "Turn-On" responses provided by only Cys through deaggregation. Furthermore, the selective deaggregation of the ensemble with Cys was well supported by background amino acid analysis as exposed in Fig. S10. In addition to PL spectra, the UV–vis spectra of **PBI**-Hg^{2+} (Fig. 6) completely returned to its original **PBI** state from 583 to 562 nm and therefore confirmed the deaggregation induced by Hg^{2+}-S interaction of Cys. Moreover, a clear isosbestic point at 571 nm (UV–vis spectra) might be arisen from Hg^{2+}-S interaction and the deaggregation. The reversible nature of **PBI**-Hg^{2+} assembly was further demonstrated by the addition of PMDTA as noticed in Fig. S11a, in which **PBI**-Hg^{2+} was completely disassociated to **PBI**. Interestingly, upon the addition of 1 equiv. of PMDTA [66,67] in THF to **PBI**-Hg^{2+}, the PL peak of **PBI** was recovered and the probe can be reusable up to 8 cycles as publicized in Fig. S11b. Hence, this result confirmed the deaggregation nature of **PBI**-Hg^{2+} linear complex assembly. The naked eye and fluorescent photographs of reversibility of **PBI**-Hg^{2+} with Cys and PMDTA were visualized in Fig. 7 and supported the deaggregation of the linear assembly. Further explanations for aggregation and deaggregation behaviors of **PBI** with Hg^{2+} and Cys will be provided by the ^1H NMR titrations in Section 3.6.

3.5. Fluorescence titrations on Cysteine

To evaluate the detection range and the turn-on response by deaggregation of **PBI**-Hg^{2+} induced by Cys, further titration on Cys was carried out individually as shown in Fig. 8. Upon the addition

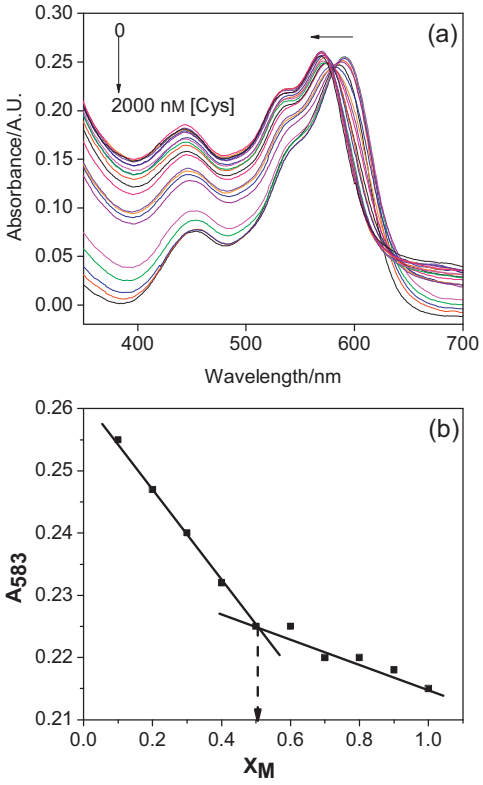

Fig. 6. (a) UV–vis spectra of **PBI**-Hg^{2+} as a function of Cys (0.1–2 μM) (b) Job plots of **PBI**-Hg^{2+}+Cys; X_M = [Cys]/[Cys] + **PBI**-Hg^{2+}, **PBI**-Hg^{2+}+Cys = 1:1 stoichiometry (ca. 0.514).

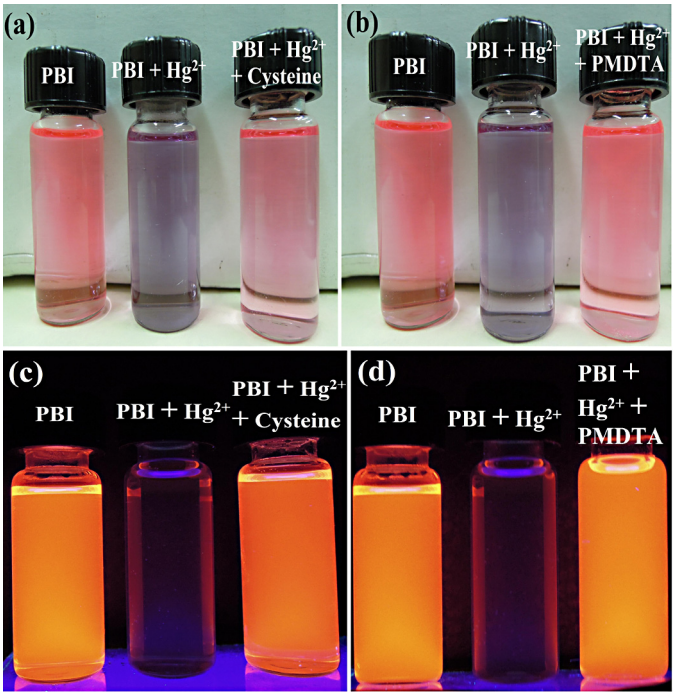

Fig. 7. Naked eye and fluorescence (under UV-light irradiations; λ = 365 nm) photographs for deaggregation and reversibilities of **PBI**-Hg^{2+} with Cys (a and c) and PMDTA (b and d).

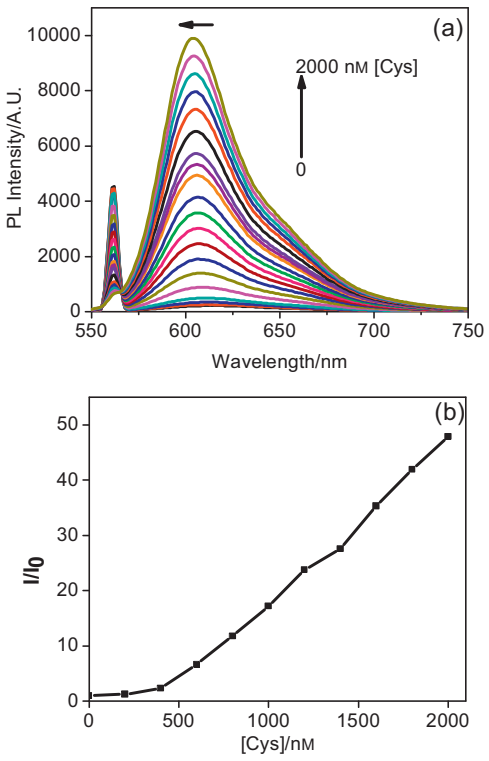

Fig. 8. (a) Fluorescence intensity changes of **PBI**-Hg^{2+} ensemble in THF:H_2O (2:1) with 0.1–2 μM addition of Cys in H_2O and (b) relative fluorescence intensity changes of PBI-Hg^{2+} as a function of [Cys] (λ_{ex} = 562 nm).

of Cys (0–2 μM with an equal span of 0.1 μM), the **PBI** monomeric peak slowly appeared with a hypsochromic shift from 612 to 591 nm. In addition, the deaggregation of **PBI**-Hg^{2+} was further confirmed by the isoemission point at 565 nm in PL spectra. However, the above observation was also clarified by UV–vis absorption spectra (Fig. 6), in which the peak hypsochromically shifted from 583 to 562 nm. Interestingly, the restored imide —NH peak in ^{1}H NMR titrations by the addition of Cys was well supported the deaggregation of **PBI**-Hg^{2+} ensemble to **PBI**. Furthermore, the deaggregation of **PBI**-Hg^{2+} were verified by the colorimetric shift and fluorescence enhancements as evidenced by Fig. 7a and c.

3.6. *Stoichiometry and ^{1}H NMR titrations [68–71]*

To ensure both sensor responses of **PBI**+Hg^{2+} and **PBI**-Hg^{2+}+Cys, their stoichiometries were calculated through job's plots as noticed in Figs. 5b and 6b. The job's plots for mole fraction (X_M) and UV–vis spectral changes at 583 nm went through maxima at molar fractions of ca. 0.503 (**PBI**+Hg^{2+}) and 0.514 (**PBI**-Hg^{2+}+Cys), which hence confirmed the 1:1 stoichiometry in both cases. Moreover, the 1:1 stoichiometry of both systems were further supported by ^{1}H NMR titrations as noticed in Fig. 9. Assuming the 1:1 stoichiometry of **PBI**-Hg^{2+} ensemble, initially 1 equiv. (10 mmol) of Hg^{2+} in D_2O was slowly added to 1 equiv. (10 mmol) of **PBI** as shown in Fig. 9a. Due to the formation of linear *J*-aggregated complex assembly, the imide —NH peak disappeared utterly with broadened spectral peaks of remaining proton environment. The —NH proton peak showed a downfield shift from 8.46 to 8.76 ppm during the titrations, which might be arisen from the linear *J*-aggregated complex assembly of **PBI**-Hg^{2+}. The above conceptual statement was also well supported through —NH peak disappearance in IR spectrum (Fig. S8d). Similar to the ^{1}H NMR titration results of **PBI** with Hg^{2+}, the addition of Cys to **PBI**-Hg^{2+} ensemble provided the incredible spectral change via a restored imide —NH peak along with the

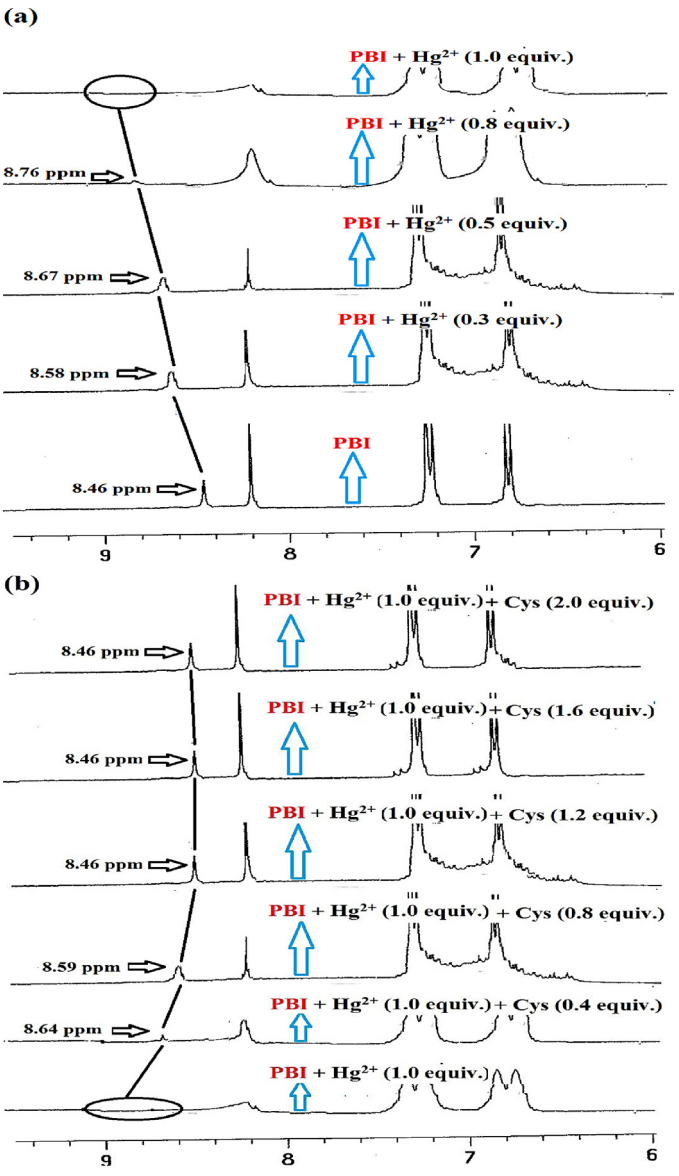

Fig. 9. ^{1}H NMR titrations of (a) **PBI** (10 mmol) with Hg^{2+} (10 mmol) ions and (b) PBI-Hg^{2+} ensemble with Cys (10 mmol).

remaining proton environment as exposed in Fig. 9b. During the addition of Cys (10 mmol), the imide —NH and other **PBI** peaks were slowly restored and hence confirmed the deaggregation of **PBI**-Hg^{2+} and 1:1 stoichiometry as well.

3.7. Hill plots and detection limits (LODs) [72,73]

As reported by Jiang et al., we also calculated the apparent association constants ($\log K_{app}$) for **PBI**-Hg^{2+} and **PBI**-Hg^{2+}+Cys by using $\log[Y/(1-Y)] = n\log[G] + \log K_{app}$ equation, where Y, n, $[G]$, and K_{app} represent the fraction of ligand binding sites filled, Hill coefficient, concentration of guest (here Hg^{2+} or Cys), and the apparent association constant, respectively. Y was determined by the equation of $(I-I_0)/(I_{max}-I_0)$, where I_0, I and I_{max} are the fluorescence intensity at 612 nm in the absence, in the presence, and in the presence of an excess amount of Hg^{2+}. Similar to the assembled interaction of complex **PBI**-Hg^{2+}, I_0, I and I_{max} of ensemble **PBI**-Hg^{2+}+Cys showed fluorescence intensity changes at 591 nm in the absence, in the presence and in the presence of an excess amount of Cys, respectively. By plotting $\log[Y/(1-Y)]$ with respect to $\log[Hg^{2+}]$

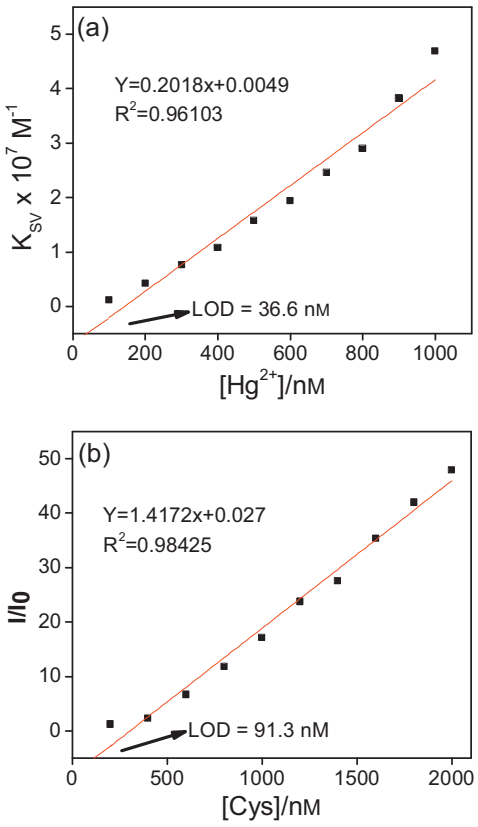

Fig. 10. Calculations of detection limits (LODs) for (a) Hg^{2+} (**PBI**-Hg^{2+}) and (b) Cys (**PBI**-Hg^{2+}+Cys) by standard deviations and linear fittings.

or log [Cys], the apparent association constants were calculated as noticed in Fig. S12. As shown in Table 1, $\log K_{app}$ for Hg^{2+} and Cys were found to be 27.7 and 9.2, respectively, and in both cases we observed positive cooperativities ($n > 1$) as well. On the other hand, the detection limits (LODs) of both sensor responses were calculated by standard deviations and linear fittings of K_{SV} (for Hg^{2+}) and relative PL intensity (I/I_0) changes (for Cys) as functions of Hg^{2+} (0–1000 nM) and Cys (0–2000 nM) concentrations. The LODs of Hg^{2+} and Cys were calculated as 36.6 and 91.3 nM, respectively as noticed in Fig. 10 and Table 1. Contrast to Jiang et al. report, the lower detection limits of Hg^{2+} and Cys might be attributed to a different kind of aggregation exhibited by **PBI**-Hg^{2+} ensemble. However, naked eye detections of both Hg^{2+} and Cys by **PBI** was an added advantage in our report.

3.8. pH, time, quantum yield (Φ) and TRPL spectra [74–80]

Since many sensor responses were affected by pH values, we extended our Hg^{2+} sensor analysis in that direction as shown in Figs. 11a and S13. In contrast to **PBI** in different pH values (Figs. 11a and S13), the **PBI**+Hg^{2+} ensemble was affected by acidic and basic pHs (Figs. 11a and S13b), and Hg^{2+} sensor was incredibly active between pHs 6–8. Therefore, we performed all our sensor analysis toward Hg^{2+} and Cys at pH = 7. Assuming the 1:1 stoichiometry of Hg^{2+} in **PBI**-Hg^{2+} and Cys in **PBI**-Hg^{2+}+Cys, the time effects (0–180 s) on both sensors were evaluated. After 1 equiv. addition of Hg^{2+} within 60 s, the PL peak of **PBI** was completely quenched. However, upon the addition of Cys to **PBI**-Hg^{2+} ensemble, a monomeric **PBI** peak slowly appeared between 0 and 120 s as shown in Fig. S14. In addition to pH and time effects on both sensor responses, the quantum yield (Φ) of **PBI** was also affected by the additions of Hg^{2+} and Cys/PMDTA sequentially as shown

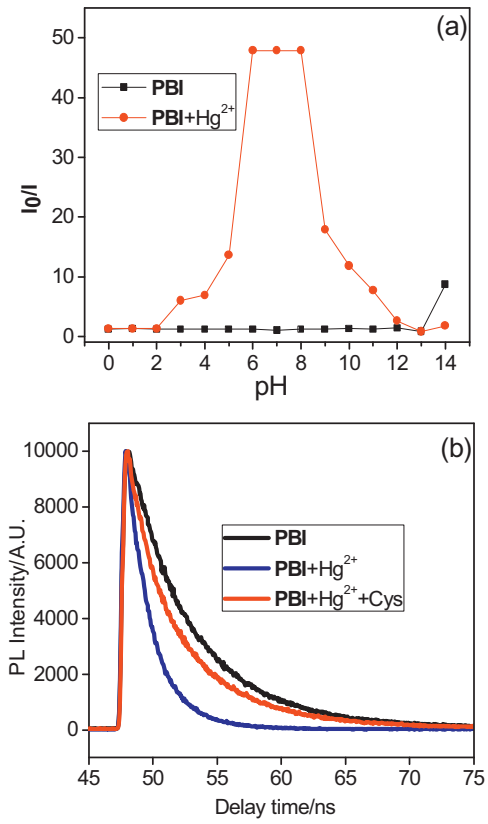

Fig. 11. (a) **PBI** and **PBI**+Hg^{2+} as functions of pH values and (b) TRPL spectra of **PBI**, **PBI**+Hg^{2+}, and **PBI**+Hg^{2+}+Cys (λ_{ex} = 562 nm).

in Table 1. The initial Φ value of **PBI** (Φ = 0.55) was 18 times quenched by Hg^{2+} (Φ = 0.03 in **PBI**-Hg^{2+}) and restored to its original stage with Cys (Φ = 0.52 in **PBI**-Hg^{2+}+Cys) or PMDTA (Φ = 0.53 in **PBI**-Hg^{2+}+PMDTA), which hence further confirmed the aggregation and deaggregation of **PBI** with Hg^{2+} and Cys, respectively. As exposed in Fig. 11b, time resolved photoluminescence (TRPL) spectra of **PBI** were influenced by Hg^{2+} and restored with Cys, and their TRPL spectral and sensor properties are summarized in Tables 1 and S2. Based on single exponential decay fittings, the average decay constant (τ) value of **PBI** (5.59 ns) was decreased in **PBI**-Hg^{2+} (2.37 ns) and further recovered in **PBI**-Hg^{2+}+Cys (5.16 ns)/**PBI**-Hg^{2+}+PMDTA (5.37 ns). Furthermore, the TRPL spectra of **PBI**-Hg^{2+} and **PBI**-Hg^{2+}+PMDTA also supported the reversibility of the Hg^{2+} sensor response as shown in Fig. S15b. Additionally, Fig. S15a and Table S2 also verified a moderate selectivity of **PBI** toward Ag^{+}.

4. Conclusions

A 1,6,7,12-tetra(4-*tert*-butylphenoxy)perylene-3,4:9,10-tetracarboxylic acid bisimide (**PBI**) derivative is reported as Hg^{2+} ions and Cysteine (Cys) naked eye and fluorescent sensors for the first time via *J*-aggregation and deaggregation mechanisms. The 1:1 stoichiometric aggregation of linear complex assembly **PBI**-Hg^{2+} and dissociation of monomeric ensemble **PBI**-Hg^{2+}+Cys were elucidated by the measurements of UV–vis/PL, ^{1}H NMR, and FT-IR. More interestingly, the Hg^{2+} sensor was reusable up to 8 cycles and hence confirmed the deaggregation possibility of **PBI**-Hg^{2+}. The positive cooperativities of **PBI**-Hg^{2+} and Cys-Hg^{2+}/**PBI** ensembles were evidenced by the Hill plots to have the log K_{app} values of 27.7 and 9.2, respectively. The detection limits of Hg^{2+} ions and Cys were estimated as 36.6 and 91.3 nM, respectively, by standard deviations and linear fittings, and the K_{SV} value of Hg^{2+} was calculated as $4.68 \times 10^{7}\ M^{-1}$. The sensor properties of **PBI** are well supported by the pH, time, quantum yield (Φ), and TRPL studies in this report.

Acknowledgment

The authors thank the National Science Council of Taiwan (ROC) through NSC101-2113-M-009-013-MY2 for the financial support.

Appendix A. Supplementary data

Supplementary data associated with this article can be found, in the online version, at http://dx.doi.org/10.1016/j.snb.2013.12.082.

References

[1] B. Valeur, I. Leray, Design principles of fluorescent molecular sensors for cation recognition, Coord. Chem. Rev. 205 (2000) 3–40.
[2] H.H. Harris, I. Pickering, G.N. George, The chemical form of mercury in fish, Science 301 (2003) 1203.
[3] R.K. Mahajan, R. Kaur, V. Bhalla, M. Kumar, T. Hattori, S. Miyano, Mercury(II) sensors based on calix[4]arene derivatives as receptor molecules, Sens. Actuators B: Chem. 130 (2008) 290–294.
[4] H.N. Kim, W.X. Ren, J.S. Kim, J. Yoon, Fluorescent and colorimetric sensors for detection of lead, cadmium, and mercury ions, Chem. Soc. Rev. 41 (2012) 3210–3244.
[5] F. Wang, S.W. Nam, Z. Guo, S. Park, J. Yoon, A new rhodamine derivative bearing benzothiazole and thiocarbonyl moieties as a highly selective fluorescent and colorimetric chemodosimeter for Hg^{2+}, Sens. Actuators B: Chem. 161 (2012) 948–953.
[6] F.D. Natale, A. Lancia, A. Molino, M.D. Natale, D. Karatza, D. Musmarra, Capture of mercury ions by natural and industrial materials, J. Hazard. Mater. 132 (2006) 220–225.
[7] N.J. Wang, C.M. Sun, W.S. Chung, A specific and ratiometric chemosensor for Hg^{2+} based on triazole coupled ortho-methoxyphenylazocalix[4]arene, Tetrahedron 67 (2011) 8131–8139.
[8] S. Park, W. Kim, K.M.K. Swamy, H.Y. Lee, J.Y. Jung, G. Kim, Y. Kim, S.J. Kim, J. Yoon, Rhodamine hydrazone derivatives bearing thiophene group as fluorescent chemosensors for Hg^{2+}, Dyes Pigments 99 (2013) 323–328.
[9] P.B. Tchounwou, W.K. Ayensu, N. Ninashvili, D. Sutton, Environmental exposure to mercury and its toxicopathologic implications for public health, Environ. Toxicol. 18 (2003) 149–175.
[10] R. Eisler, Health risks of gold miners: a synoptic review, Environ. Geochem. Health 25 (2003) 325–345.
[11] I. Onyido, A.R. Norris, E. Buncel, Biomolecule–mercury interactions: modalities of DNA base-mercury binding mechanisms. Remediation strategies, Chem. Rev. 104 (2004) 5911–5929.
[12] A. Ono, H. Togashi, Highly selective oligonucleotide-based sensor for mercury(II) in aqueous solutions, Angew. Chem. Int. Ed. 43 (2004) 4300–4302.
[13] R. Martınez, A. Espinosa, A. Tarraga, P. Molina, A new bis(pyrenyl)azadiene-based probe for the colorimetric and fluorescent sensing of Cu(II) and Hg(II), Tetrahedron 66 (2010) 3662–3667.
[14] K.H. Chu, Y. Zhou, Y. Fang, L.H. Wang, J.Y. Li, J. Yao, Rhodamine-pyrene conjugated chemosensors for ratiometric detection of Hg^{2+} ions: different sensing behavior between a spirolactone and a spirothiolactone, Dyes Pigments 98 (2013) 339–346.
[15] T.W. Clarkson, L. Magos, G.J. Myers, The toxicology of mercury – current exposures and clinical manifestations, New Engl. J. Med. 349 (2003) 1731–1737.
[16] C. He, W. Zhu, Y. Xu, T. Chen, X. Qian, Trace mercury(II) detection and separation in serum and water samples using a reusable bifunctional fluorescent sensor, Anal. Chim. Acta 651 (2009) 227–233.
[17] C.M.L. Carvalho, E.H. Chew, S.I. Hashemy, J. Lu, A. Holmgren, Enzyme catalysis and regulation, J. Biol. Chem. 283 (2008) 11913–11923.
[18] Z. Guo, J. Duan, F. Yang, M. Li, T. Hao, S. Wang, D. Wei, A test strip platform based on DNA-functionalized gold nanoparticles for on-site detection of mercury(II) ions, Talanta 93 (2012) 49–54.
[19] W.F. Fitzgerald, C.H. Lamborg, C.R. Hammerschmidt, Marine biogeochemical cycling of mercury, Chem. Rev. 107 (2007) 641–662.
[20] M.H. Keefe, K.D. Benkstein, J.T. Hupp, Luminescent sensor molecules based on coordinated metals: a review of recent developments, Coord. Chem. Rev. 205 (2000) 201–228.
[21] E.M. Nolan, S.J. Lippard, Tools and tactics for the optical detection of mercuric ion, Chem. Rev. 108 (2008) 3443–3480.
[22] J. Du, M. Hu, J. Fan, X. Peng, Fluorescent chemodosimeters using mild chemical events for the detection of small anions and cations in biological and environment media, Chem. Soc. Rev. 41 (2012) 4511–4535.

[23] (a) B. Liu, H. Tian, A selective ratiometric fluorescent chemodosimeter for mercury ion, Chem. Commun. (2005) 3156–3158;
(b) J.F. Chang, Y. Zhou, J. Yoon, J.S. Kim, Recent progress in fluorescent and colorimetric for detection of precious metal ions (silver gold, and platinum ions), Chem. Soc. Rev. 40 (2011) 3416–3429.
[24] (a) X. Wu, J. Chen, J.X. Zhao, A reversible fluorescent logic gate for sensing mercury and iodide ions based on a molecular beacon, Analyst 138 (2013) 5281–5287;
(b) Z.G. Wang, J. Elbaz, I. Williner, DNA machines: bipedal walker and stepper, Nano Lett. 11 (2011) 304–309.
[25] P.K. Sudeep, S.T.S. Joseph, K.G. Thomas, Selective detection of cysteine and glutathione using gold nanorods, J. Am. Chem. Soc. 127 (2005) 6516–6517.
[26] H.Y. Shiu, H.C. Chong, Y.C. Leung, M.K. Wong, C.M. Che, A highly selective fret-based fluorescent probe for detection of cysteine and homocysteine, Chem. Eur. J. 16 (2010) 3308–3313.
[27] L. Shang, S.J. Dong, Sensitive detection of cysteine based on fluorescent silver clusters, Biosens. Bioelectron. 24 (2009) 1569–1573.
[28] C. Zheng, S. Pu, G. Liu, B. Chen, Y. Dai, A highly selective colorimetric sensor for cysteine and homocysteine based on a new photochromic diarylethene, Dyes Pigments 98 (2013) 280–285.
[29] H. Refsum, P.M. Ueland, O. Nygard, S.E. Vollset, Homocysteine and cardiovascular disease, Annu. Rev. Med. 49 (1998) 31–62.
[30] S. Shahrokhian, Lead phthalocyanine as a selective carrier for preparation of a cysteine-selective electrode, Anal. Chem. 73 (2001) 5972–5978.
[31] S. Seshadri, A. Beiser, J. Selhub, P.F. Jacques, I.H. Rosenberg, R.B.D. Agostino, P.W.F. Wilson, Plasma homocysteine as a risk factor for dementia and Alzheimer's disease, New Engl. J. Med. 346 (2002) 476–483.
[32] Y. Yue, Y. Guo, J. Xu, S. Shao, A bodipy-based derivative for selective fluorescence sensing of homocysteine and cysteine, New J. Chem. 35 (2011) 61–64.
[33] Z. Guo, S.W. Nam, S. Park, J. Yoon, A highly selective ratiometric near-infrared fluorescent cyanine sensor for cysteine with remarkable shift and its application in bioimaging, Chem. Sci. 3 (2012) 2760–2765.
[34] W.H. Wang, O. Rusin, X.Y. Xu, K.K. Kim, J.O. Escobedo, S.O. Fakayode, K.A. Fletcher, M. Lowry, C.M. Schowalter, C.M. Lawrence, F.R. Fronczek, I.M. Warner, R.M. Strongin, Detection of homocysteine and cysteine, J. Am. Chem. Soc. 127 (2005) 15949–15958.
[35] Z.A. Wood, E. Schroder, J.R. Harris, L.B. Poole, Structure, mechanism and regulation of peroxiredoxins, Trends Biochem. Sci. 28 (2003) 32–40.
[36] M. Zhang, M. Yu, F. Li, M. Zhu, M. Li, Y. Gao, L. Li, Z. Liu, J. Zhang, D. Zhang, T. Yi, C. Huang, A highly selective fluorescence turn-on sensor for cysteine/homocysteine and its application in bioimaging, J. Am. Chem. Soc. 129 (2007) 10322–10323.
[37] Q. Li, Y. Guo, S. Shao, A BODIPY based fluorescent chemosensor for Cu(II) ions and homocysteine/cysteine, Sens. Actuator B: Chem. 171–172 (2012) 872–877.
[38] X. Zeng, X. Zhang, B. Zhu, H. Jia, Y. Li, A highly selective wavelength-ratiometric and colorimetric probe for cysteine, Dyes Pigments 94 (2012) 10–15.
[39] D.T. Quang, J.S. Kim, Fluoro- and chromogenic chemodosimeters for heavy metal ion detection in solution and biospecimens, Chem. Rev. 110 (2010) 6280–6301.
[40] D.L. Ma, V.P.Y. Ma, D.S.H. Chan, K.H. Leung, H.Z. He, C.H. Leung, Recent advances in luminescent heavy metal complexes for sensing, Coord. Chem. Rev. 256 (2012) 3087–3113.
[41] G. Sivaraman, T. Anand, D. Chellappa, Development of a pyrene based *turn on* fluorescent chemosensor for Hg^{2+}, RSC Adv. 2 (2012) 10605–10609.
[42] X. Chen, Y. Zhou, X. Peng, J. Yoon, Fluorescent and colorimetric probes for detection of thiol, Chem. Soc. Rev. 39 (2010) 2120–2135.
[43] M.S.T. Goncalves, Fluorescent labeling of biomolecules with organic probes, Chem. Rev. 109 (2009) 190–212.
[44] Z. Yan, S. Guang, H. Xu, X. Liu, An effective real-time colorimeteric sensor for sensitive and selective detection of cysteineunder physiological conditions, Analyst 136 (2011) 1916–1921.
[45] K. Liu, L. He, X. He, Y. Guo, S. Shao, S. Jiang, Calix[4]pyrrole-TCBQ assembly: a signal magnifier of TCBQ for colorimetric determining amino acids and amines, Tetrahedron Lett. 48 (2007) 4275–4279.
[46] M. Zhu, M. Yuan, X. Liu, J. Xu, J. Lv, C. Huang, H. Liu, Y. Li, S. Wang, D. Zhu, Visible near-infrared chemosensor for mercury ion, Org. Lett. 10 (2008) 1481–1484.
[47] X. Chen, S.W. Nam, M.J. Jou, Y. Kim, S.J. Kim, S. Park, J. Yoon, Hg^{2+} Selective fluorescent and colorimetric sensor: its crystal structure and application to bioimaging, Org. Lett. 10 (2008) 5235–5238.
[48] W.C. Lin, C.Y. Wu, Z.H. Liu, C.Y. Lin, Y.P. Yen, A new selective colorimetric and fluorescent sensor for Hg^{2+} and Cu^{2+} based on a thiourea featuring a pyrene unit, Talanta 81 (2010) 1209–1215.
[49] N. Kaur, S. Kumar, Colorimetric metal ion sensors, Tetrahedron 67 (2011) 9233–9264.
[50] Y. Zhou, J. Yoon, Recent progress in fluorescent and colorimetric chemosensors for detection of amino acids, Chem. Soc. Rev. 41 (2012) 52–67.
[51] H. Su, Q. Zheng, H. Li, Colorimetric detection and separation of chiral tyrosine based on *N*-acetyl-L-cysteine modified gold nanoparticles, J. Mater. Chem. 22 (2012) 6546–6548.
[52] Q. Li, Y. Guo, S. Shao, A bodipy based fluorescent chemosensor for Cu(II) ions and homocysteine/cysteine, Sens. Actuator B: Chem. 171–172 (2012) 872–877.
[53] F. Miao, J. Zhan, Z. Zou, D. Tian, H. Li, A new Hg^{2+} fluorescent sensors based on 1,3-alternate thiacalix[4] arene (L) and the complex of [L+Hg^{2+}] as turn-on sensor for cysteine, Tetrahedron 68 (2012) 2409–2413.
[54] D. Siegel, Applications of reversible covalent chemistry in analytical sample preparation, Analyst 137 (2012) 5457–5482.
[55] Y.B. Ruan, A.F. Li, J.S. Zhao, J.S. Shen, Y.B. Jiang, Specific Hg^{2+}-mediated perylene bisimide aggregation for highly sensitive detection of cysteine, Chem. Commun. 46 (2010) 4938–4940.
[56] X. Zheng, D. Zhang, D. Zhu, A new tetrathiafulvalene-perylene diimide dyad with a pentaoxa-heptadecane chain as the spacer:metal-ions-induced aggregation, Tetrahedron Lett. 47 (2006) 9083–9087.
[57] Y. Che, X. Yang, L. Zang, Ultraselective fluorescent sensing of Hg^{2+} through metal coordination-induced molecular aggregation, Chem. Commun. (2008) 1413–1415.
[58] S. Yagai, T. Seki, T. Karatsu, A. Kitamura, F. Wurthner, Transformation from H- to J-aggregated perylene bisimide dyes by complexation with cyanurates, Angew. Chem. Int. Ed. 47 (2008) 3367–3371.
[59] F. Wurthner, T.E. Kaiser, C.R. Saha-Moller, J-aggregates: from serendipitous discovery to supramolecular engineering of functional dye materials, Angew. Chem. Int. Ed. 50 (2011) 3376–3410.
[60] Y.C. Rajan, S. Muthaiah, C.T. Huang, H.C. Lin, H.C. Lin, Synthesis of novel supramolecular triads bearing a H-bonded perylene bisimide core, Tetrahedron 68 (2012) 7926–7931.
[61] R.A. Robinson, R.H. Stokes, Electrolyte Solutions, 2nd ed. Rev., Butterworth, London, 1968.
[62] F. Wurthner, C. Thalacker, A. Sautter, W. Schartl, W. Ibach, O. Hollricher, Hierarchical self-organization of perylene bisimide-melamine assemblies to fluorescent mesoscopic superstructures, Chem. Eur. J. 6 (2000) 3871–3886.
[63] J.H. Hurenkamp, W.R. Browne, R. Augulis, A. Pugzlys, P.H.M. van Loosdrecht, J.H. van Esch, B.L. Feringa, Intramolecular energy transfer in a tetra-coumarin perylene system: influence of solvent and bridging unit on electronic properties, Org. Biomol. Chem. 5 (2007) 3354–3362.
[64] M. Queste, C. Cadiou, B. Pagoaga, L. Giraudet, N. Hoffmann, Synthesis and characterization of 1,7-disubstituted and 1,6,7,12-tetrasubstituted perylenetetracarboxy-3,4:9,10-diimide derivatives, New J. Chem. 34 (2010) 2537–2545.
[65] M.R. Silva-Junior, W.J. Thiel, Benchmark of electronically excited states for semi-empirical methods: MNDO, AM1, PM3, OM1, OM2, OM3, INDO/S, and INDO/S2, Chem. Theory Comput. 6 (2010) 1546–1564.
[66] H.C. Chu, Y.H. Lee, S.J. Hsu, P.J. Yang, A. Yabushita, H.C. Lin, Novel reversible chemosensory material based on conjugated side-chain polymer containing fluorescent pyridyl receptor pendants, J. Phys. Chem. B 115 (2011) 8845–8852.
[67] P.J. Yang, H.C. Chu, T.C. Chen, H.C. Lin, Recoverable fluorescence chemosensors for Ni^{2+} ions based on hydrogenbonded side-chain copolymers presenting pendent benzoic acid and pyridyl receptor units, J. Mater. Chem. 22 (2012) 12358–12368.
[68] S. Muthaiah, Y.C. Rajan, H.C. Lin, Synthesis of novel triarylamine-based dendrimers with N^4,N^6-dibutyl-1,3,5-triazine-4,6-diamine probe for electron/energy transfers in H-bonded donor–acceptor–donor triads and as efficient Cu^{2+} sensors, J. Mater. Chem. 22 (2012) 8976–8987.
[69] G. Sivaraman, T. Anand, D. Chellappa, Turn-on fluorescent chemosensor for Zn(II) via ring opening of rhodamine spirolactam and their live cell imaging, Analyst 137 (2012) 5881–5884.
[70] W. Zhou, Y. Li, Y. Li, H. Liu, S. Wang, C. Li, M. Yuan, X. Liu, D. Zhu, Pyrene-based dual-mode fluorescence switches and logic gates that function in solution and film, Chem. Asian J. 1–2 (2006) 224–230.
[71] S. Muthaiah, Y.H. Wu, H.C. Lin, Simple pyridyl-salicylimine-based fluorescence turn on sensors for distinct detections of Zn^{2+}, Al^{3+} and OH^- ions in mixed aqueous media, Analyst 138 (2013) 2931–2942.
[72] S. Shinkai, M. Ikeda, A. Sugasaki, M. Takeuchi, Positive allosteric systems designed on dynamic supramolecular scaffolds: toward switching and amplification of guest affinity and selectivity, Acc. Chem. Res. 34 (2001) 494–503.
[73] S. Muthaiah, Y.H. Wu, A. Singh, M.V.R. Raju, H.C. Lin, Novel pyrene- and anthracene-based Schiff base derivatives as Cu^{2+} and Fe^{3+} fluorescence turn-on sensors and for aggregation induced emissions, J. Mater. Chem. A 1 (2013) 1310–1318.
[74] B. Ma, F. Zeng, F. Zheng, S. Wu, A fluorescence turn-on sensor for iodide based on a thymine-Hg^{II}-thymine complex, Chem. Eur. J. 17 (2011) 14844–14850.
[75] M. Hecht, W. Kraus, K. Rurack, A highly fluorescent pH sensing membrane for the alkaline pH range incorporating a BODIPY dye, Analyst 138 (2013) 325–332.
[76] G. Zhang, D. Zhang, S. Yin, X. Yang, Z. Shuai, D. Zhu, Phosphine ligand triggered oxidative decarbonylative homocoupling of aromatic aldehydes: selectively generating biaryls and diarylketones, Chem. Commun. (2005) 2161–2163.
[77] S.K. Arya, S. Bhansali, Lung cancer and its early detection using biomarker-based biosensors, Chem. Rev. 111 (2011) 6783–6809.
[78] Q. Zhao, F. Li, C. Huang, Phosphorescent chemosensors based on heavy-metal complexes, Chem. Soc. Rev. 39 (2010) 3007–3030.
[79] M.H. Ha-Thi, M. Penhoat, D. Drouin, M. Blanchard-Desce, V. Michelet, I. Leray, Synthesis, fluorescence, and two-photon absorption of bidentate phosphane oxide derivatives: complexation with Pb^{2+} and Cd^{2+} cations, Chem. Eur. J. 14 (2008) 5941–5950.
[80] M. Schaferling, The art of fluorescence imaging with chemical sensors, Angew. Chem. Int. Ed. 51 (2012) 3532–3554.

Biographies

Hsiao-Ping Fang received her B.S. in chemical engineering from I-Shou University, M.S. in chemistry from Fu Jen University, Ph.D. in materials science and engineering

from National Chiao Tung University and was working on photovoltaic polymers and nanocomposites for energy transfer and solar cell materials.

Muthaiah Shellaiah received his M.Phil. in synthetic organic chemistry from University of Madras, Chennai. Completed his Ph.D. and had a post-doctoral experience (5 months) under the supervision of Prof Hong-Cheu Lin at the National Chiao Tung University, Taiwan (ROC) and is working on chemosensors and hydrogen bonded supramolecular complexes.

Ashutosh Singh received his M.Sc. in chemistry from C. S. J. M. University, Kanpur. Currently, he is a Ph.D. student under the supervision of Prof Hong-Cheu Lin at the National Chiao Tung University, Taiwan (ROC) and is working on small molecule and polymeric chemosensors.

Mandapati V. Ramakrishnam Raju received his M.Sc. in organic chemistry from Andhra University, Visakhapatnam. Completed his Ph.D. and currently working as a post-doctoral fellow under the supervision of Prof. Hong-Cheu Lin at National Chiao Tung University, Taiwan (ROC) and is working on functional mechanically interlocked molecules, such as rotaxanes, catenanes, and novel drug delivery of snap-top vehicles with an emphasis on supramolecular interactions for diagnostic applications.

Yen-Hsing Wu received his M.Sc. in chemical engineering from Chung Yuan Christian University. Currently, he is a Ph.D. student under the supervision of Prof. Hong-Cheu Lin at National Chiao Tung University, Taiwan (ROC) and is working on photovoltaic polymers and nanocomposites for energy transfer and solar cell materials.

Hong-Cheu Lin received his B.S. in chemical engineering from National Taiwan University, M.S. in chemical engineering from Northwestern University, Ph.D. in materials science and engineering from University of Illinois at Urbana-Champaign. Currently, he is a Professor and vice-director of department of materials science and engineering at National Chiao Tung University, Taiwan (ROC). He is working on various supramolecular materials and nano-composites for electro-optical applications (such as liquid crystals), as well as organic semiconductors for light emitters, solar cells, and thin film transistors (as chemo- and bio-sensors).